Journal of Materials Chemistry A

ROYAL SOCIETY OF CHEMISTRY

PAPER

View Article Online
View Journal | View Issue

Cite this: J. Mater. Chem. A, 2020, 8, 17780

Hexane isomers separation on an isoreticular series of microporous Zr carboxylate metal organic frameworks†

Adriano Henrique, [ab] Tanmoy Maity,[c] Hengli Zhao,[de] Pedro F. Brântuas, [b] Alírio E. Rodrigues, [a] Farid Nouar,[f] Aziz Ghoufi, [d] Guillaume Maurin,*[e] José A. C. Silva*[b] and Christian Serre *[f]

A series of isoreticular Zr carboxylate MOFs, MIL-140A, B and C, exhibiting 1D microporous triangular shaped channels and based on different aromatic dicarboxylate ligands (1,4-BDC, 2,6-NDC and 4,4′-BPDC, respectively), were investigated by chromatographic breakthrough experiments regarding their ability to separate hexane isomers (nC6/2MP/3MP/23DMB/22DMB). Both single and equimolar multicomponent experiments were performed at the temperatures 343, 373, and 423 K and a total hydrocarbon pressure up to 50.0 kPa using the MIL-140B form. The elution order is similar to that of the normal boiling point of the compounds nC6 > 2MP > 3MP > 23DMB > 22DMB. It is noteworthy that this material enables separation of the hexane isomers by class, linear > mono-branched > di-branched, with a selectivity (linear + mono-branched isomers/di-branched isomers) up to 10 at 343 K, decreasing, however, as the temperature increases. Grand canonical Monte Carlo simulations were further performed to gain insight into the adsorption/separation mechanisms, highlighting the crucial need to consider a tiny tilting of the organic linkers for capturing the experimental observations. The impact of the pore size was finally assessed through the comparison with MIL-140A and MIL-140C, respectively, based on multicomponent experiments at 343 K. We evidenced a significant decrease of the selectivity (about 2) in both cases while the loadings were decreased or increased for MIL-140A and MIL-140C, respectively. Additionally, MIL-140C was demonstrated to exhibit an uncommon shift in the elution order occurring between nC6 and 3MP, 3MP being the last compound to saturate in the column.

Received 2nd June 2020
Accepted 30th July 2020

DOI: 10.1039/d0ta05538g

rsc.li/materials-a

1. Introduction

There is increasing consensus to enhance fuel quality in order to minimize its negative impacts on the environment and public health.[1–3] As a result, restrictions have been imposed on gasoline production, limiting the concentration of toxic additives, such as aromatic and olefin compounds, along with the removal of lead.[4] Therefore, the petrochemical industry has been searching for alternatives to enhance the required octane number in gasoline.

In this context, the process of isomerization has gained significant attention for the treatment of light straight-run naphtha (LSRN) for the octane improvement of gasoline pools.[5–7] Normal paraffins are catalytically converted into their branched isomers with a higher Research Octane Number (RON). Therefore, the linear pentane (nC5, RON: 61.8) is isomerized to produce isopentane (iC5, RON: 92.3), while the linear *n*-hexane (nC6: RON 24.8) is rearranged into 3-methylpentane (3MP: RON 74.5), 2-methylpentane (2MP: RON 73.4), 2,3-dimethylbutane (23DMB: RON 101.7) and 2,2-

[a]Laboratory of Separation and Reaction Engineering, Laboratory of Catalysis and Materials (LSRE/LCM), Department of Chemical Engineering, Faculty of Engineering University of Porto, Rua Dr. Roberto Frias, S/N, 4200-465 Porto, Portugal

[b]Centro de Investigação de Montanha (CIMO), Instituto Politécnico de Bragança, Campus de Santa Apolónia, 5300-253 Bragança, Portugal. E-mail: jsilva@ipb.pt

[c]Solid State and Structural Chemistry Unit, Indian Institute of Science, Bangalore, Karnataka 560012, India

[d]Univ. Rennes, CNRS, IPR (Institut de Physique de Rennes) – UMR 6251, F-35000 Rennes, France

[e]ICGM, Univ. Montpellier, CNRS, ENSCM, Montpellier, France. E-mail: guilaume.maurin1@umontpellier.fr

[f]Institut des Matériaux Poreux de Paris, Ecole Normale Supérieure de Paris, ESPCI Paris, CNRS, PSL University, 75005 Paris, France. E-mail: christian.serre@ens.fr

† Electronic supplementary information (ESI) available: Characterization of MIL-140s: powder X-ray diffraction, infrared spectroscopy, thermogravimetric analysis, gas sorption study, and surface study on MIL-140B; sampling of MIL-140s; simulation details and results: force field: alkane model, MIL-140B model, grand canonical Monte Carlo simulations, adsorption isotherms and radial distribution functions; experimental conditions for measuring breakthrough curves of hexane isomers on MIL-140s; multicomponent breakthrough curves of hexane isomers on MIL-140B; selectivities of hexane isomers on MIL-140B; and impact of the pore size. See DOI: 10.1039/d0ta05538g

dimethylbutane (22DMB: RON 91.8).[8,9] However, this reaction is limited by the thermodynamic equilibrium, and so the product still contains around 10% of unreacted linear and 50% of mono-branched paraffins.[10] Thus, the Total Isomerization Process – TIP[11,12] – employs zeolite 5A to separate the final product in a fraction composed of only branched isomers, with a final RON around 87–90, recycling the linear paraffins back to the reactor.[8,11,12] To achieve a further improvement of the average RON, the separation of mono-branched hexanes (2MP/3MP) is desirable to obtain a rich fraction of di-branched hexane isomers (23DMB/22DMB) as products. For this purpose, extensive efforts are being made to find alternative adsorbents that would be able to selectively separate branched hexane isomers.

Over the past two decades, porous crystalline hybrid solids such as Metal Organic Frameworks (MOFs) have been extensively studied for a wide range of potential applications, including adsorption and separation, catalysis, sensing, biomedicine, *etc.*[13–16] MOFs could be of great interest in separating acetylene from ethylene,[17,18] propane from propylene,[19,20] xylene isomers,[21,22] carbon dioxide from methane[23–25] or nitrogen,[26–28] carbon monoxide from hydrogen or nitrogen,[29] and acetylene from carbon dioxide,[30] among others.[31–35] Regarding the separation of hexane isomers, several MOFs have been considered to date.[36–46] For instance ZIF-8, featuring a sodalite zeolite type structure, can completely remove *n*-hexane from branched isomers with higher adsorption capacity than zeolite 5A.[40–42] $Fe_2(BDP)_3$, consisting in a framework of one-dimensional triangular channels that can accommodate all hexane isomers, separates them by the degree of branching.[43] Mendes *et al.*[44] demonstrated by ternary breakthrough experiments (22DMB/3MP/nC6) that the flexible MOF MIL-53(Fe)-$(CF_3)_2$ is able to discriminate mono from di-branched paraffins *via* kinetic mechanisms at low temperatures. Recently, Wang and co-workers reported two interesting MOFs composed of 1D channels: the zirconium-based MOF $Zr_6O_4(OH)_8(-H_2O)_4(abtc)_2$, which shows a thermodynamically controlled separation of hexane isomers by class,[45] and the calcium-based MOF Ca(H_2-tcpb), which exhibits a unique molecular exclusion behavior of di-branched hexanes enabling the separation of hexane isomers into the pure form of each isomerate.[46]

MOFs are attractive candidates for adsorptive applications since their structure, pore size, shape and composition can be systematically varied by a judicious choice of metal ions and/or bridging organic linkers. A prominent example of this tunability is the isoreticular series of MOFs such as microporous MIL-140 materials,[47] constructed from zirconium oxide sub-units and aromatic dicarboxylate ligands, featuring a general formula of $[ZrO(O_2C–R–CO_2)]$ with R = C_6H_4, $C_{10}H_6$, $C_{12}H_8$ and $C_{12}N_2H_6Cl_2$ for MIL-140A, MIL-140B, MIL-140C and MIL140D, respectively (MIL stands for Materials from Institut Lavoisier). These materials exhibit one-dimensional triangular shaped microporous channels with pore sizes of roughly 3.2, 4.0, 5.7 and 6.3 Å for MIL-140A, MIL-140B, MIL-140C and MIL140D, associated with BET surface areas from 350 $m^2\ g^{-1}$ up to 1000 $m^2\ g^{-1}$, respectively. In addition, these solids show a pronounced hydrophobic character and a high hydrothermal and a good mechanical stability.[47]

To date, to the best of our knowledge, only two computational studies[39,43] have recently been reported on the adsorption of hexane isomers in this isoreticular MIL-140 series revealing that these materials are not expected to show attractive separation performances. However, these conclusions merit reconsideration since these calculations were performed using a rigid framework, a critical assumption when one deals with the adsorption of bulky molecules in small pore MOFs. This encouraged us to conduct an unprecedented experimental exploration of the sorption of hexane isomers on the MIL-140 series. Moreover, it was shown in the literature from breakthrough experiments that structures featuring one-dimensional triangular channels are appealing for separating the hexane isomers by class.[43] Since the average pore aperture of the MIL-140 series covers the range of kinetic diameters of hexane isomers, 4.3–6.2 Å, the study of this series is of high interest.

Therefore, the main objective of this work was to evaluate the potential of microporous MIL-140 (A, B and C) for the separation of hexane isomers. For MIL-140B, the most promising material, the adsorption behavior was explored in depth by measuring not only adsorption equilibrium isotherms but also single and multicomponent breakthrough curves, exploiting the effect of temperature and total hydrocarbon pressure. Additionally, force field grand canonical Monte Carlo simulations were further performed to shed light on the experimental adsorption data of all hexane isomers in MIL-140B. Regarding MIL-140A and C, screening tests addressing multicomponent experiments were performed, their selectivities being compared with the ones obtained for MIL-140B.

2. Experimental section

2.1. Synthesis of MIL-140s

For the preparation of all MIL-140 solids the following chemicals were used: zirconium chloride ($ZrCl_4$, Alfa Aesar, 99.5+ %), terephthalic acid ($C_8H_6O_4$, Sigma-Aldrich, 98%), 2,6-naphthalenedicarboxylic acid ($C_{12}H_8O_4$, Alfa Aesar, 98%), biphenyl-4,4′-dicarboxylic acid ($C_{14}H_{12}O_4$, Acros Organics, 98%) and acetic acid ($C_2H_4O_2$, Merck). All solvents, *N*,*N*-dimethylformamide (C_3H_7NO), ethanol (C_2H_6O), methanol (CH_4O), and acetone (C_3H_6O), used for synthesis and purification were purchased from Merck.

For all MIL-140s, the synthesis parameters were adapted from previously reported conditions:[47]

MIL-140A: 1.18 g (10 mmol) of $ZrCl_4$ and 1.68 g (10 mmol) terephthalic acid were mixed with 32 mL dimethylformamide solvent and placed inside a 125 mL Teflon autoclave. The autoclave was heated at 493 K for 12 h. After cooling to room temperature, the mixture was recovered by centrifugation and the solid material was stirred with methanol overnight and dried in a vacuum oven.

MIL-140B: 0.7 g (3 mmol) of $ZrCl_4$, 1.26 g (6 mmol) 2,6-naphthalene dicarboxylic acid and 342 μL (6 mmol) acetic acid were mixed with 15 mL dimethylformamide solvent and placed inside a 125 mL Teflon autoclave. The autoclave was heated at 493 K for 7 h. After cooling to room temperature, the mixture

was recovered by centrifugation and the solid material was stirred with methanol overnight and dried in a vacuum oven.

MIL-140C: 1.17 g (5 mmol) of $ZrCl_4$, 2.42 g (10 mmol) 4,4′-biphenyl dicarboxylic acid and 1430 μL (25 mmol) acetic acid were mixed with 25 mL dimethylformamide solvent and placed inside a 125 mL Teflon autoclave. The autoclave was heated at 493 K for 12 h. After cooling to room temperature, the mixture was recovered by centrifugation and the solid material was stirred with methanol overnight and dried in a vacuum oven.

2.2. Characterization of MIL-140s

All the synthesized MOFs were fully characterized by laboratory powder X-ray diffraction (PXRD, $\lambda CuK\alpha_{1,2}$), infrared spectroscopy (IR), thermogravimetric analysis (TGA) under a nitrogen atmosphere, and nitrogen adsorption measurements at 77 K in order to understand the porous nature of MIL-140A, B and C MOFs. In addition, the MIL-140B sample was further characterized by scanning electron microscopy (SEM) for surface study. Complete information about the characterization procedures is given in ESI S1.†

2.3. Sampling of MIL-140s

Prior to adsorption experiments, powdered MIL-140 solids were transformed into small agglomerates (see ESI S2†) to minimize diffusion issues. First, the powdered solids were compacted into tablets in a hydraulic press machine; the pressure applied was 6.5 kg mm^{-2}. Thereafter, the tablets were broken into small fragments and sieved to produce a known particle size distribution of around 2.5 mm. After packing the adsorption column, the materials were activated for 12 h at 473 K under a pure helium flow.

2.4. Experimental setup and procedure

The equilibrium adsorption data were measured using apparatus developed at the CIMO for measuring single and multicomponent breakthrough curves in a fixed bed. The experimental set-up consisted of three main sections: (1) a gas preparation, (2) an adsorption, and (3) an analytical section. In the gas preparation section, the paraffin hydrocarbon (in the liquid phase) is continuously introduced with a syringe pump in the carrier gas to run through a vaporizer, located in the preparative chromatograph. The adsorption section consists in a stainless-steel column with a 0.1 m length and 0.004 m internal diameter, entirely filled with adsorbent material and placed inside the preparative chromatograph oven. The output stream of the packed column is constantly monitored using a thermal conductivity detector. The analytical section is composed of an analytical chromatograph, a capillary GC column coating (Supelco with a 15 m length, 0.1 mm outer diameter and 0.1 μm poly(dimethyl sulfoxane)) immersed in an ice water bath, and a Flame Ionization Detector (FID).

The experimental procedure to obtain single and multicomponent breakthrough curves consists of continuously measuring the concentration profile of the paraffin hydrocarbon as a function of time at the outlet of the adsorption column, at a particular partial pressure and temperature. The equilibrium loading (amount adsorbed) is determined by integrating the concentration profiles of the breakthrough curve. A more detailed description about the experimental setup and procedure has already been reported elsewhere.[41,42] For the whole adsorption study, all paraffin isomers (nC6/2MP/3MP/23DMB/22DMB) were of analytical grade and supplied by Sigma Aldrich with 99+ % purity.

2.5. Molecular simulations

Single-component and equimolar quinary mixture adsorption isotherms for all paraffin isomers were predicted by grand canonical Monte Carlo (GCMC) simulation for MIL-140B. These calculations were carried out at 343 K using a simulation box made of a $1 \times 2 \times 4$ unit cell of the MIL-140B crystal structure[47] with atoms fixed in their initial positions. The alkanes were treated using the uncharged united-atom TraPPE model[48,49] while each atom of MIL-140B was considered a single Lennard-Jones site associated with parameters taken from the generic UFF[50] and Dreiding[51] force fields. The hexane isomers/MIL-140B interactions were described by a Lennard-Jones (LJ) potential with cross-term LJ parameters derived using the Lorentz Berthelot mixing rule. The cutoff distance was set to 12 Å. The simulation consisted of 5×10^5 Monte Carlo steps for equilibration and 4×10^6 Monte Carlo steps for production. Additional Monte Carlo simulations in the NVT ensemble were considered to explore the preferential adsorption sites and calculate the radial distribution functions between hexane isomers/MOF atom pairs. All details of the calculations are provided in ESI S3.†

3. Results and discussion

3.1. Single component adsorption of hexane isomers on MIL-140B

Single component breakthrough curves of nC6, 2MP, 3MP, 23DMB and 22DMB in a fixed bed of MIL-140B were measured at three different temperatures, 343 K, 373 K and 423 K, and a total hydrocarbon pressure up to 50.0 kPa. Helium was used to set-up a total pressure in the column of 101.3 kPa. Complete information on the experimental fixed bed runs performed, including the flow-rates of hydrocarbon and helium, and also the equilibrium loading for each run are detailed in Table S4.1 (see ESI S4†). One can observe that the adsorption equilibrium hierarchy of hexane isomers on MIL-140B always fits the following trend: nC6 > 2MP > 3MP > 23DMB > 22DMB, being similar to the normal boiling point order of the components.

The corresponding adsorption isotherms are shown in Fig. 1. Whatever the temperature studied, all isotherms are of type I, characteristic of microporous adsorbents.[52] Additionally, a clear tendency for separating the hexane isomers by class, linear (nC6) > mono-branched (2MP/3MP) > di-branched (23DMB/22DMB), is expected especially at low hydrocarbon partial pressures. It is noteworthy that this experimental observation drastically deviates from the conclusions drawn from the molecular simulations previously reported by Dubbeldam *et al.*[39] stating the adsorption of only linear and mono-branched isomers.

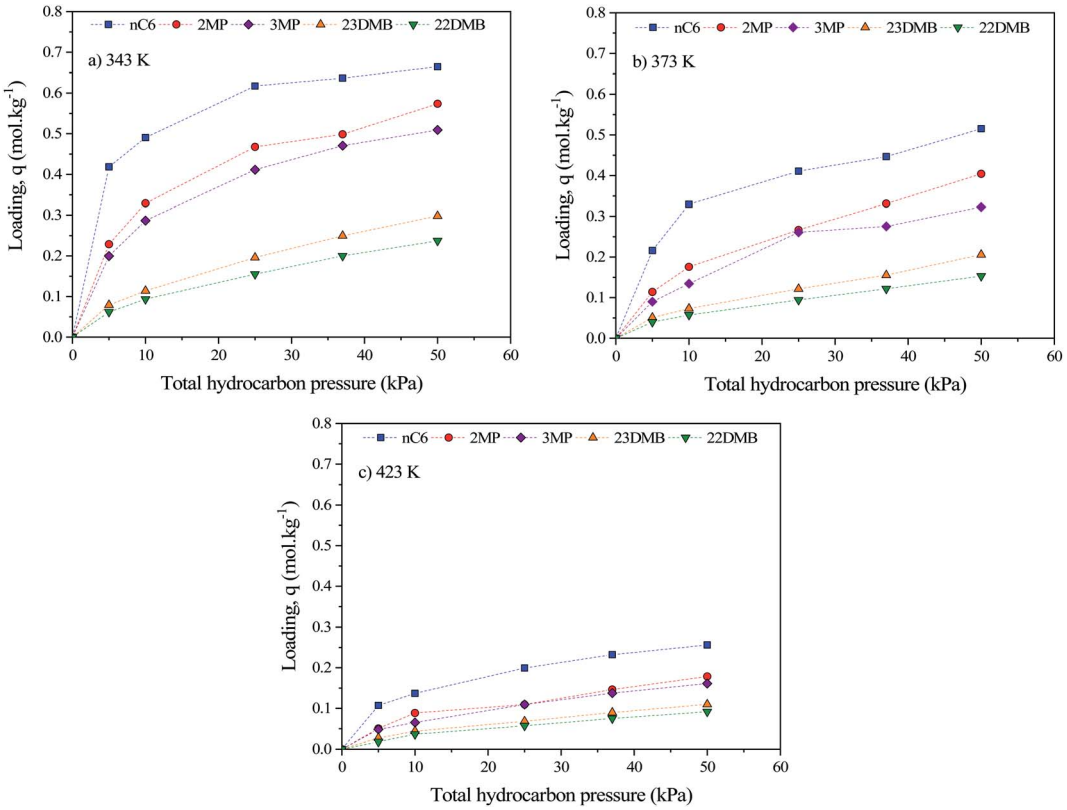

Fig. 1 Experimental adsorption equilibrium isotherms of hexane isomers on MIL-140B at (a) 343 K, (b) 373 K, and (c) 423 K.

GCMC simulations were thus further performed to gain insight into the adsorption of all hexane isomers in MIL-140B. We first observed that the simulated adsorption isotherms significantly overestimate the corresponding experimental data for all isomers in the whole range of pressures (Fig. S3.4†). This result clearly confirms that the approximation of a rigid model

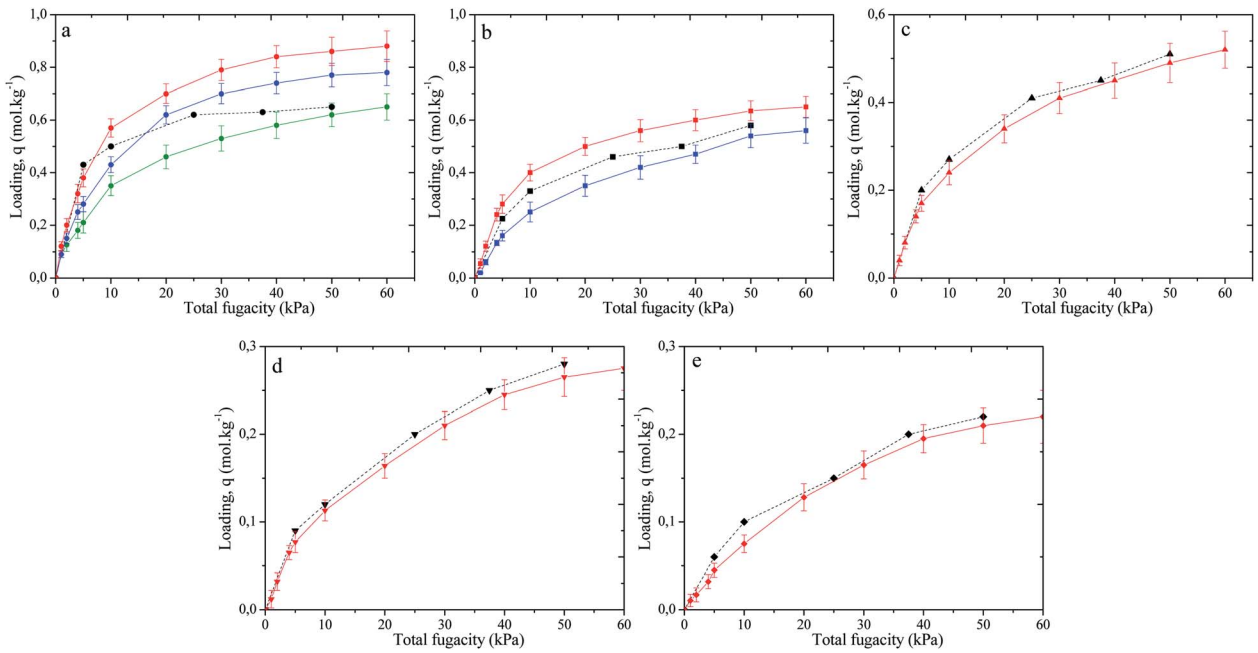

Fig. 2 Simulated and experimental single component adsorption isotherms at 343 K: (a) nC6 -●- experimental data, -●- 5° linker rotation, -●- 7° linker rotation, and -●- 10° linker rotation; (b) 2MP -■- experimental data, -■- 6° linker rotation, and -■- 7° linker rotation; (c) 3 MP -▲- experimental data and -▲- 1° linker rotation; (d) 23DMB -▼- experimental data and -▼- 4° linker rotation; and (e) 22DMB -◆- experimental data and -◆- 4° linker rotation.

for the host framework that has been applied by Dubbeldam *et al.*[39] can hardly be applied to study the adsorption of bulky molecules in ultra-microporous MOFs like MIL-140B.

Indeed a guest-induced reorientation of the linker that has already been reported for many MOFs[53,54] is expected to impact the adsorption uptakes for the architectures with the smallest pore size, this becoming even more valid for the bulkier molecules like with the hexane isomers. To confirm this assumption, a series of MIL-140B configurations were constructed by systematically tilting all the organic linkers by a maximum of 15° and their corresponding adsorption isotherms were simulated (Fig. S3.5–S3.9†). Fig. 2 reveals that a relatively small tilting below 10° allows the reproduction of the experimental adsorption isotherms for all isomers. Typically, Fig. 2a and b show that the experimental profiles for nC6 and 2MP cannot be reproduced by considering a single tilted configuration. This emphasizes that the degree of reorientation of the organic linker slightly changes upon incremental adsorption, the experimental adsorption isotherm being mostly described as a composite of 2 or 3 simulated adsorption isotherms obtained for distinct MIL-140B configurations. In the case of 3MP and the di-branched alkanes, we observe an overall good agreement with the consideration of 2° and 4° tilted configurations, respectively.

Fig. 3 further illustrates the preferential sittings of each isomer in the most representative tilted MIL-140B configurations. The loading for nC6, 2MP and 3MP corresponds to 1 molecule per unit cell while 0.5 molecules per unit cell are considered for 22DMB and 23DMB. The molecules are arranged in such a way as to interact with the organic linkers preferentially *via* their $-CH_3$ united atoms. This implies relatively weak van der Waals interactions with characteristic separation MOF/hexane isomer distances over 3 Å (see † S3.12†). A decreasing sequence of the isosteric heats of adsorption was predicted *i.e.* 54.6 kJ mol^{-1}, 51.2 kJ mol^{-1}, 47.5 kJ mol^{-1}, 44.4 kJ mol^{-1}, and 41.3 kJ mol^{-1} for nC6, 2MP, 3MP, 22DMB and 23DMB, following the experimental trend for the adsorption uptakes at low pressure.

3.2. Multicomponent adsorption of hexane isomers on MIL-140B

To gain further insight into the adsorption of hexane isomers in MIL-140B, multicomponent breakthrough curves were measured with an equimolar mixture of all five hexane isomers nC6/2MP/3MP/23DMB/22DMB. The experiments were performed in the same range of temperatures and total hydrocarbon pressures covered in single component experiments.

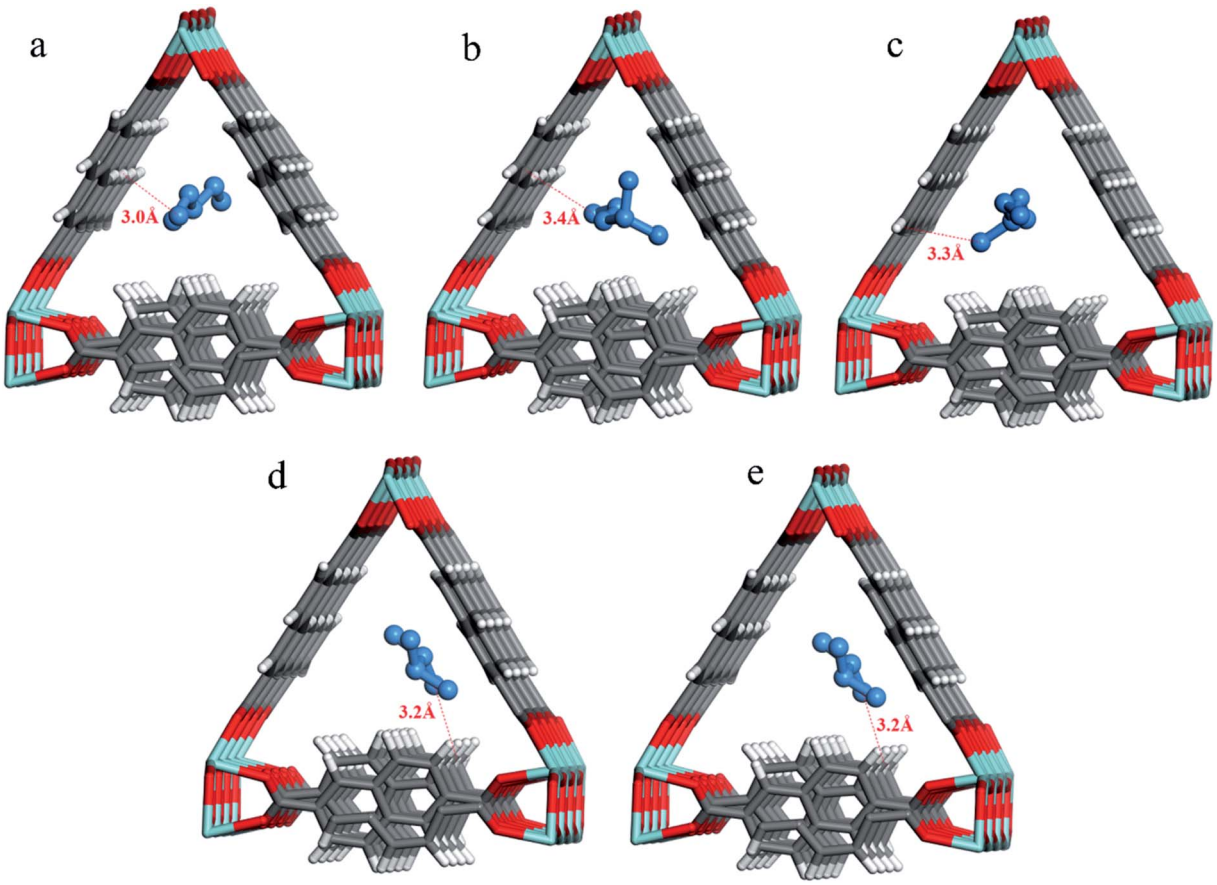

Fig. 3 Illustration of the preferential sittings of hexane isomers in the pores of MIL-140B simulated at 343 K: (a) nC6, (b) 2MP, (c) 3MP, (d) 23DMB, and (e) 22DMB. The red dashed lines represent the distance between CH_3 and H. The carbon, hydrogen, oxygen, zirconium and $-CH_x$ united atoms are represented in grey, white, red, light blue and dark blue, respectively.

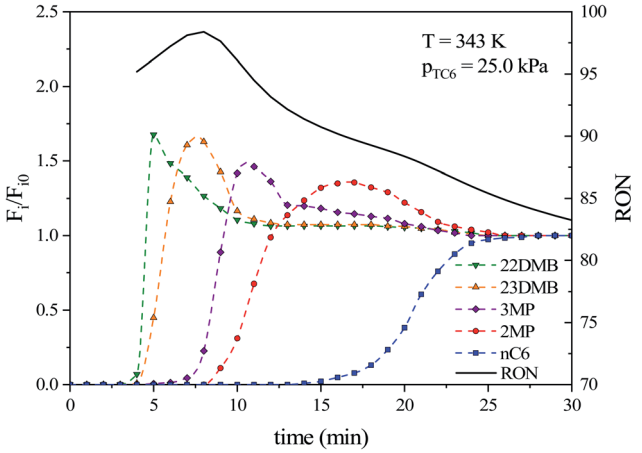

Fig. 4 Experimental multicomponent breakthrough curves for a quinary equimolar mixture of hexane isomers on MIL-140B at 343 K and 25.0 kPa. Loadings: 22DMB: 0.0180, 23DMB: 0.0249, 3MP: 0.0704, 2MP: 0.0960, and nC6: 0.254 mol kg^{-1}.

Table S4.2† summarizes all the experimental conditions applied and equilibrium loadings as well. The mixture loading follows the same thermodynamic consistence observed in single component experiments.

Fig. 4 shows the breakthrough curves for a quinary mixture of hexane isomers on MIL-140B at a fixed temperature of 343 K and total hydrocarbon pressure of 25.0 kPa. Additional information regarding the effect of hydrocarbon pressure is reported in Fig. S.51, S.52 and S.53† for the temperatures 343, 373 and 423 K, respectively. The results indicate that the sorption hierarchy of hexane isomers in MIL-140B is always nC6 > 2MP > 3MP > 23DMB > 22DMB, consistent with single component experiments. Moreover, at the lowest temperature of 343 K (Fig. 4 and S5.1†) one can equally observe the ability of the material to fractionate the hexane isomers based on the degree of branching: linear (nC6: 0.254 mol kg^{-1}) $\gg$ mono-branched (2MP: 0.0960 mol kg^{-1}, 3MP: 0.0704 mol kg^{-1}) $\gg$ di-branched (23DMB: 0.0249 mol kg^{-1}, 22DMB: 0.0180 mol kg^{-1}) isomers, which is of major importance to obtain high RON values. Also, the RON values increased up to 98 when only the di-branched hexanes 22DMB and 23DMB left the column separated from the other isomers. However, this sequence is strongly affected by increasing temperature, where at 423 K (Fig. S5.3†) the separation of branched isomers practically disappears. At the highest temperature, a higher magnitude and faster rotation of the organic linkers is expected to be at the origin of the less-selective behavior of MIL-140B.

In addition, in the breakthrough curves, we observe the so-called roll-up phenomenon,[55] where the least adsorbed solutes in the following hierarchical order, 22DMB < 23DMB $\ll$ 3MP < 2MP $\ll$ nC6, are then desorbed by the more strongly adsorbed ones by an adsorption equilibrium competition displacement

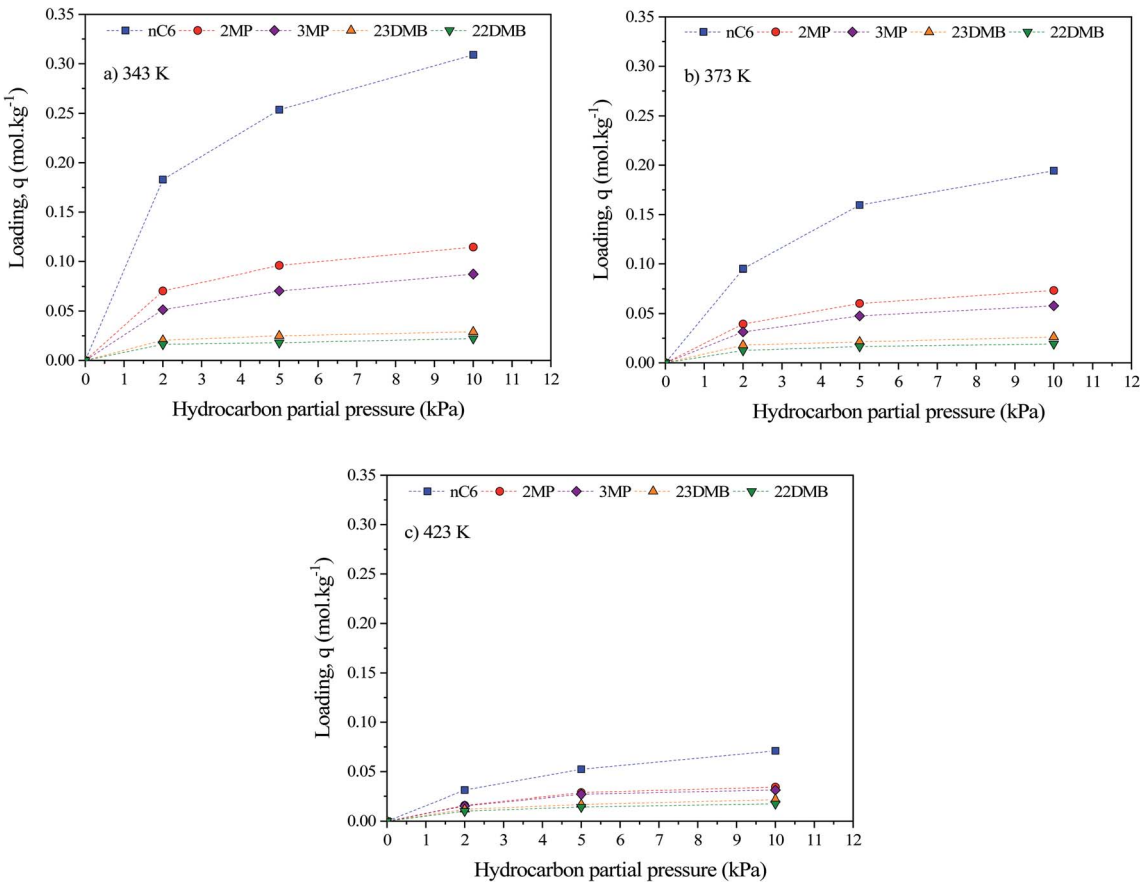

Fig. 5 Experimental equimolar quinary mixture adsorption isotherms of hexane isomers on MIL-140B at (a) 343 K, (b) 373 K, and (c) 423 K.

process. Since the least adsorbed components (moving faster in the column) are pushed off the adsorbent by the more strongly adsorbed ones (moving slower in the column), their concentration rises above that of the feed (Fig. 4 and S5.1†) in a sequential manner. In the case of the least adsorbed di-branched paraffins (22DMB and 23DMB) the rise in concentration can be 50% above the feed concentration. This phenomenon evidences the strong competition for sorption between di-branched, mono-branched, and linear paraffins, which is a major advantage for separating the hexane isomers into fractions of low and high RON ones. As the temperature increases, these overshoots in concentration become smaller, as is the case observed at a temperature of 423 K (Fig. S5.3†) since the adsorption mixture loading is smaller.

The selectivities (S_{ads}) from multicomponent experiments were measured using the ratio of the loadings between linear + mono-branched paraffins over the di-branched ones according to the following equation:[43]

$$S_{ads} = \frac{(q_{nC6} + q_{2MP} + q_{3MP})}{(q_{22DMB} + q_{23DMB})} \quad (1)$$

Fig. S6.1† displays the selectivities of hexane isomers on MIL-140B plotted as a function of total hydrocarbon pressure. They range from around 10 at 343 K to 3 at 423 K. Moreover, the selectivities remain practically constant in the range of total hydrocarbon pressures studied.

Fig. 5 shows the quinary adsorption equilibrium isotherms of hexane isomers on MIL-140B. Again, the isotherms are of type I according to IUPAC classification.[52] One can also note that, globally, the amount of linear nC6 adsorbed is around two times higher than that of branched isomers, mostly due to steric hindrance of the bulkier isomers that prevent more adsorption within the very narrow pores of MIL-140B. It is also observed that the loadings of hexane isomers are separated based on their class, linear > mono-branched > di-branched, especially at 343 K.

Grand canonical Monte Carlo simulations were also performed for multicomponent experiments on MIL-140B, being the equimolar quinary mixture adsorption isotherms calculated for typical pristine and tilted MIL-140B configurations (see Fig. S3.10 and S3.11 †). These simulated data reproduce the experimental sequence well in terms of affinity at low loading as well as in terms of uptakes nC6 > 2MP > 3MP > 23DMB > 22DMB. The selectivity calculated using eqn (1) at 10 kPa and 343 K was found be about 15.5, overestimating the experimental value. This deviation can be explained by the fact that a single tilted configuration cannot capture the whole adsorption regime of this mixture.

3.3. Impact of the pore size

Adsorption screening studies were further performed for MIL-140A and MIL-140C through multicomponent breakthrough curves with equimolar mixtures of hexane isomers at 343 K, to probe the effect of the pore size on the separation of isomers, MIL-140A having the smallest pore size and MIL-140C having the largest of the series. The experimental conditions and loadings are summarized in Table S4.3,† together with the results obtained for MIL-140B for comparison. Fig. 6a and b show the experimental breakthroughs for MIL140A and MIL-140C, respectively, at a total hydrocarbon pressure of 25 kPa. The results obtained at different total pressures (10.0 kPa and 50.0 kPa) are displayed in Fig. S7.1.†

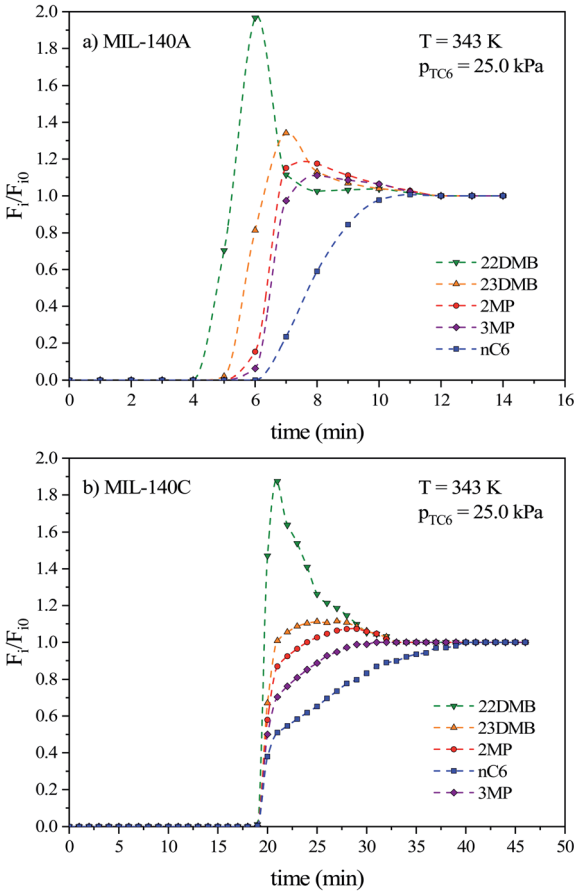

Fig. 6 Experimental multicomponent breakthrough curves for a quinary equimolar mixture of hexane isomers at 343 K and 25.0 kPa on (a) MIL-140A, loadings: 22DMB: 0.0461, 23DMB: 0.0654, 3MP: 0.0802, 2MP: 0.0754, and nC6: 0.102 mol kg^{-1} and (b) MIL-140C, loadings: 22DMB: 0.233, 23DMB: 0.284, 3MP: 0.361, 2MP: 0.297, and nC6: 0.318 mol kg^{-1}.

MIL-140A and MIL-140C cannot separate the hexane isomers with the same degree of selectivity as that exhibited by MIL-140B as depicted in Fig. 7. The selectivity values are much smaller for MIL-140A and MIL-140C (around 2) compared to MIL-140B (around 10). Furthermore, the experiments performed on MIL-140A (Fig. 6a) show a sorption hierarchy following the order of the normal boiling point of the compounds, nC6 (0.102 mol kg^{-1}) > 3MP (0.0802 mol kg^{-1}) ≥ 2MP (0.0754 mol kg^{-1}) > 23DMB (0.0654 mol kg^{-1}) ≥ 22DMB (0.0461 mol kg^{-1}), but without a pronounced separation by class as observed for MIL-140B. The mixture loading is 0.369 mol kg^{-1} in MIL-140A which is comparable to the 0.463 mol kg^{-1} for MIL-140B. It should be noted that these experimental findings again contradict the previous

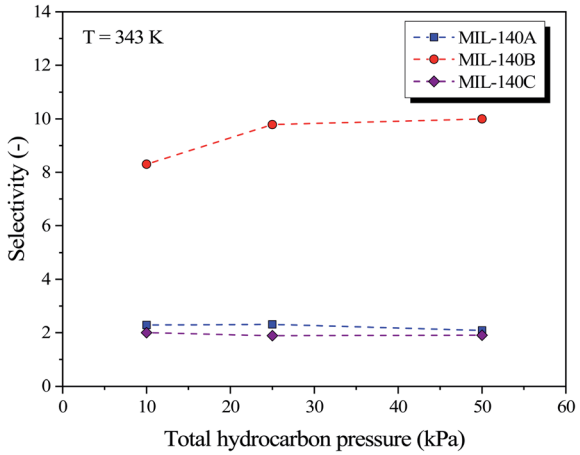

Fig. 7 Comparison between experimental multicomponent sorption selectivities of hexane isomers on MIL-140s at 343 K as a function of total hydrocarbon pressure.

simulations[39,43] stating that none of the hexane isomers can be adsorbed in MIL-140A.

Regarding MIL-140C a completely different picture is obtained. Fig. 6b shows that all hexane isomers elute practically at the same time, but with a different profile from that of saturation. This wave front (containing all the compounds) that elutes from the column after approximately 20 min is itself a separation wave front. This is uncommon behavior. A change in the order of the elution of the compounds relative to the order of the normal boiling point of the isomers is observed, where 3MP is the last component to saturate in the column. In other words, there is a shift between 3MP and nC6 in the order of elution. Consequently, the sorption hierarchy is 3MP (0.361 mol kg^{-1}) > nC6 (0.318 mol kg^{-1}) > 2 MP (0.297 mol kg^{-1}) > 23DMB (0.284 mol kg^{-1}) > 22DMB (0.233 mol kg^{-1}) which drastically differs from the sequence predicted by the two previous molecular simulation studies[39,43] (23DMB ≈ 3MP ≈ 2MP ≈ nC6 ≈ 22DMB). This suggests the critical role of the linker rotation in the sorption properties of MIL-140C even if its pore size is significantly larger than those of the A- and B-analogues. Finally, the loading of the hexane isomers in MIL-140C is much higher than the ones observed in MIL-140A and MIL-140B. Table S4.3† indicates a mixture loading of around 1.5 mol kg^{-1} in MIL-140C, which is more than twice the uptakes obtained for MIL-140A and MIL-140B. This trend is consistent with its much higher S_{BET} (780 m^2 g^{-1}) and cumulative pore volume (0.30 cm^3 g^{-1}) (see Table S1.1†) that facilitates the adsorption of all isomers, especially the di-branched ones.

4. Conclusions

We report here the first experimental study on the sorption of hexane isomers (nC6/2MP/3MP/23DMB/22DMB) in the isoreticular series of Zr oxide dicarboxylate MOFs, MIL-140s (A, B, and C). Single and multicomponent (equimolar) breakthrough curves and multicomponent equilibrium data demonstrated that MIL-140B can separate the hexane isomers by class, linear (nC6) > mono-branched (2MP, 3MP) > di-branched (23DMB, 22DMB), at low temperature (343 K) together with a high selectivity up to 10 as well as a sorption hierarchy similar to the normal boiling point order of the compounds: nC6>2MP > 3MP > 23DMB>22DMB. At higher temperature the separation progressively disappears. The specific behavior of MIL-140B was explained through a revisited molecular simulation approach that identified the microscopic origin of the hexane isomer separation, mostly governed by a slight tilting of the organic spacer as well as specific host–guest interactions. The flexibility of the organic linkers was proven to be crucial in order to reproduce the experimental trend. Finally, the impact of the pore size and the nature of the organic spacer was assessed on MIL-140A and MIL-140C. The smaller pore size MIL-140A showed a hexane isomer sorption hierarchy according to the normal boiling point order of the compounds while the larger pore size MIL-140C exhibited a mixed sorption hierarchy. In both cases, much lower selectivities were, however, observed. MIL-140C exhibited a much larger sorption capacity as well as a very uncommon shift in the elution order between 3MP and nC6 which will be the subject of molecular simulations implementing a fully flexible force field in the near future. Finally, concerning potential strategies for octane number enhancement (separation between di-branched isomers and the mono/linear ones) the results obtained with MIL-140B are encouraging especially at 343 K with a clear trend for separation by class.

Conflicts of interest

There are no conflicts to declare.

Acknowledgements

We acknowledge the financial support from (1) the project with ref POCI01-0145-FEDER-016517 (PTDC/QEQ-PRS/3599/2014) funded by the FEDER through COMPETE2020 and the FCT; (2) the project POCI-01-0145-FEDER006984-Associate Laboratory LSRE-LCM funded by the ERDF through COMPETE2020, Programa Operacional Competitividade e Internacionalização (POCI), and national funds through the FCT – Fundação para a Ciência e a Tecnologia; (3) the Foundation for Science and Technology (FCT, Portugal) and the ERDF under Programme PT2020 to the CIMO (UID/AGR/00690/2019); (4) the FCT PhD scholarship to Adriano Henrique (SFRH/BD/148525/2019); and (5) the ANR Project MEACOPA (H. Z., A. G., G. M., C. S., and F. N.).

References

1 M. P. Walsh, *Am. J. Ind. Med.*, 2007, **50**, 853–860.
2 Y. Shen, S. Shuai, J. Wang and J. Xiao, *J. Environ. Sci.*, 2009, **21**, 1208–1213.
3 G. A. Westphal, J. Krahl, T. Brüning, E. Hallier and J. Bünger, *Toxicology*, 2010, **268**, 198–203.
4 D. Swick, A. Jaques, J. C. Walker and H. Estreicher, *Regul. Toxicol. Pharmacol.*, 2014, **70**, S80–S92.

5 G. Valavarasu and B. Sairam, *Pet. Sci. Technol.*, 2013, **31**, 551–562.
6 S. R. Naqvi, A. Bibi, M. Naqvi, T. Noor, A.-S. Nizami, M. Rehan and M. Ayoub, *Appl. Petrochem. Res.*, 2018, **8**, 131–139.
7 A. Aitani, M. N. Akhtar, S. Al-Khattaf, Y. Jin, O. Koseoglo and M. T. Klein, *Energy Fuels*, 2019, **33**, 3828–3843.
8 N. A. Cusher, in *Handbook of Petroleum Refining Processes*, ed. R. A. Meyers, McGraw-Hill, New York, 3rd edn, 2004, pp. 9.29-9.39.
9 D. Sullivan, S. Metro and P. R. Pujadó, in *Handbook of Petroleum Processing*, ed. S. A. Treese, P. R. Pujadó and D. S. J. Jones, Springer International Publishing Switzerland, Switzerland, 2014.
10 D. Peralta, G. Chaplais, A. Simon-Masseron, K. Barthelet and G. D. Pirngruber, *Ind. Eng. Chem. Res.*, 2012, **51**, 4692–4702.
11 T. C. Holcombe, *US Pat.*, 4176053, 1979.
12 T. C. Holcombe, *US Pat.*, 4210771, 1980.
13 R. J. Kuppler, D. J. Timmons, Q. R. Fang, J. R. Li, T. A. Makal, M. D. Young, D. Yuan, D. Zhao, W. Zhuang and H. C. Zhou, *Coord. Chem. Rev.*, 2009, **253**, 3042–3066.
14 H. Furukawa, K. E. Cordova, M. O'Keeffe and O. M. Yaghi, *Science*, 2013, **341**, 1230444.
15 B. Li, H. M. Wen, Y. Cui, W. Zhou, G. Qian and B. Chen, *Adv. Mater.*, 2016, **28**, 8819–8860.
16 S. Yuan, L. Feng, K. Wang, J. Pang, M. Bosch, C. Lollar, Y. Sun, J. Qin, X. Yang, P. Zhang, Q. Wang, L. Zou, Y. Zhang, L. Zhang, Y. Fang, J. Li and H. C. Zhou, *Adv. Mater.*, 2018, **30**, 1704303.
17 S. C. Xiang, Z. Zhang, C. G. Zhao, K. Hong, X. Zhao, D. R. Ding, M. H. Xie, C. D. Wu, M. C. Das, R. Gill, K. M. Thomas and B. Chen, *Nat. Commun.*, 2011, **2**, 1–7.
18 S. Yang, A. J. Ramirez-Cuesta, R. Newby, V. Garcia-Sakai, P. Manuel, S. K. Callear, S. I. Campbell, C. C. Tang and M. Schröder, *Nat. Chem.*, 2015, **7**, 121–129.
19 E. D. Bloch, W. L. Queen, R. Krishna, J. M. Zadrozny, C. M. Brown and J. R. Long, *Science*, 2012, **335**, 1606–1610.
20 A. Cadiau, K. Adil, P. M. Bhatt, Y. Belmabkhout and M. Eddaoudi, *Science*, 2016, **353**, 137–140.
21 C. X. Yang and X. P. Yan, *Anal. Chem.*, 2011, **83**, 7144–7150.
22 R. El Osta, A. Carlin-Sinclair, N. Guillou, R. I. Walton, F. Vermoortele, M. Maes, D. De Vos and F. Millange, *Chem. Mater.*, 2012, **24**, 2781–2791.
23 L. Hamon, N. Heymans, P. L. Llewellyn, V. Guillerm, A. Ghoufi, S. Vaesen, G. Maurin, C. Serre, G. De Weireld and G. D. Pirngruber, *Dalton Trans.*, 2012, **41**, 4052–4059.
24 G. D. Pirngruber, L. Hamon, S. Bourrelly, P. L. Llewellyn, E. Lenoir, V. Guillerm, C. Serre and T. Devic, *ChemSusChem*, 2012, **5**, 762–776.
25 J. Duan, M. Higuchi, S. Horike, M. L. Foo, K. P. Rao, Y. Inubushi, T. Fukushima and S. Kitagawa, *Adv. Funct. Mater.*, 2013, **23**, 3525–3530.
26 D. Britt, H. Furukawa, B. Wang, T. G. Glover and O. M. Yaghi, *Proc. Natl. Acad. Sci. U. S. A.*, 2009, **106**, 20637–20640.
27 P. Nugent, E. G. Giannopoulou, S. D. Burd, O. Elemento, E. G. Giannopoulou, K. Forrest, T. Pham, S. Ma, B. Space, L. Wojtas, M. Eddaoudi and M. J. Zaworotko, *Nature*, 2013, **495**, 80–84.
28 Q. Yang, S. Vaesen, F. Ragon, A. D. Wiersum, D. Wu, A. Lago, T. Devic, C. Martineau, F. Taulelle, P. L. Llewellyn, H. Jobic, C. Zhong, C. Serre, G. De Weireld and G. Maurin, *Angew. Chem., Int. Ed.*, 2013, **52**, 10316–10320.
29 E. D. Bloch, M. R. Hudson, J. A. Mason, S. Chavan, V. Crocellà, J. D. Howe, K. Lee, A. L. Dzubak, W. L. Queen, J. M. Zadrozny, S. J. Geier, L. C. Lin, L. Gagliardi, B. Smit, J. B. Neaton, S. Bordiga, C. M. Brown and J. R. Long, *J. Am. Chem. Soc.*, 2014, **136**, 10752–10761.
30 R. Matsuda, R. Kitaura, S. Kitagawa, Y. Kubota, R. V. Belosludov, T. C. Kobayashi, H. Sakamoto, T. Chiba, M. Takata, Y. Kawazoe and Y. Mita, *Nature*, 2005, **436**, 238–241.
31 J. R. Li, R. J. Kuppler and H. C. Zhou, *Chem. Soc. Rev.*, 2009, **38**, 1477–1504.
32 Z. R. Herm, E. D. Bloch and J. R. Long, *Chem. Mater.*, 2014, **26**, 323–338.
33 Z. Bao, G. Chang, H. Xing, R. Krishna, Q. Ren and B. Chen, *Energy Environ. Sci.*, 2016, **9**, 3612–3641.
34 H. Li, K. Wang, Y. Sun, C. T. Lollar, J. Li and H. C. Zhou, *Mater. Today*, 2018, **21**, 108–121.
35 R. B. Lin, S. Xiang, H. Xing, W. Zhou and B. Chen, *Coord. Chem. Rev.*, 2019, **378**, 87–103.
36 Y. G. Chung, P. Bai, M. Haranczyk, K. T. Leperi, P. Li, H. Zhang, T. C. Wang, T. Duerinck, F. You, J. T. Hupp, O. K. Farha, J. I. Siepmann and R. Q. Snurr, *Chem. Mater.*, 2017, **29**, 6315–6328.
37 V. A. Solanki and B. Borah, *Ind. Eng. Chem. Res.*, 2019, **58**, 20047–20065.
38 H. Wang and J. Li, *Acc. Chem. Res.*, 2019, **52**, 1968–1978.
39 D. Dubbeldam, R. Krishna, S. Calero and A. Ö. Yazaydin, *Angew. Chem., Int. Ed.*, 2012, **51**, 11867–11871.
40 P. A. P. Mendes, A. E. Rodrigues, P. Horcajada, C. Serre and J. A. C. Silva, *Microporous Mesoporous Mater.*, 2014, **194**, 146–156.
41 A. Henrique, A. E. Rodrigues and J. A. C. Silva, *Ind. Eng. Chem. Res.*, 2019, **58**, 378–394.
42 A. Henrique, A. E. Rodrigues and J. A. C. Silva, *Sep. Purif. Technol.*, 2020, **238**, 116419.
43 Z. R. Herm, B. M. Wiers, J. A. Mason, J. M. Van Baten, M. R. Hudson, P. Zajdel, C. M. Brown, N. Masciocchi, R. Krishna and J. R. Long, *Science*, 2013, **340**, 960–964.
44 P. A. P. Mendes, P. Horcajada, S. Rives, H. Ren, A. E. Rodrigues, T. Devic, E. Magnier, P. Trens, H. Jobic, J. Ollivier, G. Maurin, C. Serre and J. A. C. Silva, *Adv. Funct. Mater.*, 2014, **24**, 7666–7673.
45 H. Wang, X. Dong, J. Lin, S. J. Teat, S. Jensen, J. Cure, E. V. Alexandrov, Q. Xia, K. Tan, Q. Wang, D. H. Olson, D. M. Proserpio, Y. J. Chabal, T. Thonhauser, J. Sun, Y. Han and J. Li, *Nat. Commun.*, 2018, **9**, 1–11.
46 H. Wang, X. Dong, E. Velasco, D. H. Olson, Y. Han and J. Li, *Energy Environ. Sci.*, 2018, **11**, 1226–1231.
47 V. Guillerm, F. Ragon, M. Dan-Hardi, T. Devic, M. Vishnuvarthan, B. Campo, A. Vimont, G. Clet, Q. Yang,

G. Maurin, G. Férey, A. Vittadini, S. Gross and C. Serre, *Angew. Chem., Int. Ed.*, 2012, **51**, 9267–9271.
48 M. G. Martin and J. I. Siepmann, *J. Phys. Chem. B*, 1998, **102**, 2569–2577.
49 M. G. Martin and J. I. Siepmann, *J. Phys. Chem. B*, 1999, **103**, 4508–4517.
50 A. K. Rappé, C. J. Casewit, K. S. Colwell, W. A. Goddard and W. M. Skiff, *J. Am. Chem. Soc.*, 1992, **114**, 10024–10035.
51 S. L. Mayo, B. D. Olafson and W. A. Goddard, *J. Phys. Chem.*, 1990, **94**, 8897–8909.
52 M. Thommes, K. Kaneko, A. V. Neimark, J. P. Olivier, F. Rodriguez-Reinoso, J. Rouquerol and K. S. W. Sing, *Pure Appl. Chem.*, 2015, **87**, 1051–1069.
53 S. Devautour-Vinot, G. Maurin, C. Serre, P. Horcajada, D. Paula da Cunha, V. Guillerm, E. de Souza Costa, F. Taulelle and C. Martineau, *Chem. Mater.*, 2012, **24**, 2168–2177.
54 J. Pires, J. Fernandes, K. Dedecker, J. R. B. Gomes, G. Pérez-Sánchez, F. Nouar, C. Serre and M. L. Pinto, *ACS Appl. Mater. Interfaces*, 2019, **11**, 27410–27421.
55 F. Helfferich and G. Klein, *Multicomponent Chromatography: Theory of Interference*, Marcel Dekker, Inc., New York, 1970.